Maneuvering Performance of a Four-Fin Bio-Inspired UUV

Jason D. Geder and Ravi Ramamurti
Lab for Computational Physics and Fluid Dynamics
Naval Research Laboratory
Washington, DC 20375

Marius Pruessner
Center for Biomolecular Science and Engineering
Naval Research Laboratory
Washington, DC 20375

John Palmisano
NOVA Research, Inc., Contractor
Naval Research Laboratory
Washington, DC 20375

***Abstract*—This paper describes the modeling and maneuvering performance of a second generation (Gen2) bio-inspired unmanned underwater vehicle (UUV) propelled by four pectoral fins. Based on both computational fluid dynamics (CFD) simulations and experimental data, we developed a UUV model that includes a representation of actively controlled curvature fin-generated forces. The vehicle model is validated by comparing open-loop simulated responses with experimentally measured responses to identical fin thrust and lift inputs. Closed-loop control algorithms, which command changes in fin kinematics, are tested on the vehicle. Comparison of experimental and simulation results for various maneuvers validates the fin and vehicle models, and demonstrates the precise maneuvering capabilities enabled by the actively controlled curvature pectoral fins. Finally, various dynamics state responses of the Gen2 vehicle are compared with those of the smaller first generation (Gen1) vehicle to evaluate the effects of vehicle changes on performance.**

Keywords—bio-inspired; UUV; pectoral fin; robotic fish; low-speed maneuvering; underwater propulsion; station-keeping

I. INTRODUCTION

There are many undersea arenas in which traditional propulsion and sensing techniques have proven effective for unmanned systems, but these have mostly been in open waters, uncluttered and with generally predictable flow dynamics. It is in the more cluttered undersea areas with fast changing currents and near-surface wave effects that much is yet to be accomplished when it comes to unmanned platforms.

Researchers seeking to improve on vehicle performance in these environments have looked to nature as an inspiration for their designs. Fish and other aquatic organisms that inhabit the types of environments where unmanned platforms could prove very useful have are effective navigators of their domains. Combinations of finned propulsion and control surface actuation, and unique sensory systems have given these organisms the tools they need to survive and thrive, and these same systems can provide scientists and engineers with the inspiration they need to greatly improve vehicle performance in difficult environments.

A number of researchers have studied the fin force production mechanisms employed by various fish species in their attempts to understand how these organisms achieve high levels of controllability in difficult environments [1][2]. Within fish swimming, articulation of the pectoral fins has been shown to produce forces and moments ideal for high-maneuverability in low-speed and hovering operations [3][4][5]. Several investigators have developed and adapted rigid and passively deforming robotic pectoral fins onto unmanned underwater vehicles (UUVs) including [6][7][8][9]. Others have pursued the development of actively controlled curvature pectoral fins including [9][10][11][12], but few have deployed these fins on UUV platforms [13][14][15].

This paper builds on previous work with actively controlled deformation pectoral fins. A first generation (Gen1) fin was designed and experimentally tested [10][16]. A two-fin and a Gen1 four-fin vehicle were designed, constructed, and tested demonstrating the capabilities of the fins as effectors of propulsion and control [15][17][18]. Based on these results a scaled up second generation (Gen2) fin and four-fin vehicle were designed and analyzed to improve performance for operation in near-shore environments where precise low-speed maneuvering is needed in the presence of obstacles and dynamically changing flow conditions [19].

This paper details the initial modeling of the Gen2 vehicle and fin dynamics using preliminary experimental results and computational fluid dynamics (CFD) simulations, and validates these models with experimental vehicle test data. Feedback control algorithms are designed and verified through experiments demonstrating the maneuvering capabilities of the Gen2 vehicle. Comparison of the Gen1 to Gen2 vehicle maneuvering performance is made, outlining the effects of changes made to the fin and vehicle.

This work was supported by the Office of Naval Research.

II. VEHICLE DESIGN AND MODEL

A. Vehicle Design

After demonstrating the performance capabilities of a 0.41 m long four-fin vehicle in [18], added payload space and greater thrust for countering currents and wave forces in near-shore environments was determined necessary [19]. After multiple design iterations, the final 1.01 m long design was reached. Fig. 1 shows this Gen2 vehicle design with its coordinate reference frames, while Fig. 2 shows the Gen2 vehicle prototype.

The Gen2 vehicle employs a water-tight cylinder for housing the lithium batteries, control electronics, and inertial measurement sensors including three-axis gyro (ITG-3200), three-axis accelerometer (ADXL345) and compass (HMC5343). The fin mounts and housings are designed to reduce drag by minimizing cross-flow through the vehicle hull. The flooded, fiberglass molded nose and tail sections are currently reserved for additional payloads and sensors. As with the Gen1 vehicle, hardware control and all computation are performed by a 16 MHz ATmega2560 microcontroller.

B. Vehicle Model

The rigid body vehicle hull is modeled separately from the elastic bending and twisting of the fins. The six degree-of-freedom (6-DOF) translational and rotational equations of motion for a rigid body are given in [20] as,

$$\begin{aligned} m\left(\left(\frac{\partial \vec{v}_0}{\partial t}\right)_r + \vec{\omega}\times\vec{v}_0 + \dot{\vec{\omega}}\times\vec{r}_G + \vec{\omega}\times\left(\vec{\omega}\times\vec{r}_G\right)\right) &= \vec{f}_0 \\ \tilde{I}_0\dot{\vec{\omega}} + \vec{\omega}\times\left(\tilde{I}_0\vec{\omega}\right) + m\vec{r}_G\times\left(\left(\frac{\partial \vec{v}_0}{\partial t}\right)_r + \vec{\omega}\times\vec{v}_0\right) &= \vec{m}_0 \end{aligned} \quad (1)$$

Here $\boldsymbol{v_0} = [u\ v\ w]^T$ is the velocity vector, $\boldsymbol{\omega} = [p\ q\ r]^T$ is the angular rate vector, $\boldsymbol{r_G} = [x_G\ y_G\ z_G]^T$ is the center of gravity position vector, $\boldsymbol{I_0}$ is the inertia tensor, $\boldsymbol{f_0} = [X\ Y\ Z]^T$ is the external force vector, and $\boldsymbol{m_0} = [K\ M\ N]^T$ is the external moment vector. Equation (1) is rewritten in matrix form as,

$$M\dot{\vec{v}} + C(\vec{v})\vec{v} + D(\vec{v})\vec{v} + \vec{g}(\vec{\eta}) = \vec{\tau} \quad (2)$$

Here $M = M_{RB} + M_A$ is the inertia matrix for rigid body and added mass, $C = C_{RB} + C_A$ is the centripetal and Coriolis matrix, $D = D_Q + D_L$ is the hydrodynamic lift and drag matrix, $\boldsymbol{g}$ is the gravitational and buoyancy vector, $\boldsymbol{\nu} = [\boldsymbol{v_0}^T\ \boldsymbol{\omega}^T]^T$ is the body-fixed linear and angular velocity vector, $\boldsymbol{\eta} = [x\ y\ z\ \varphi\ \theta\ \psi]^T$ is the earth-fixed position and orientation vector, and $\boldsymbol{\tau} = \boldsymbol{\tau}_{fins} + \boldsymbol{\tau}_{external}$ is a vector of all forces and moments external to the rigid body.

The Gen2 vehicle hull is symmetric about the *x*-*z* and *y*-*z* planes, and although it is not symmetric about the *x*-*y* plane, it is assumed to be symmetric because it operates at low-speeds [21]. We can therefore simplify both M_{RB} and M_A to diagonal matrices, eliminating the cross-terms. Also because of vehicle symmetry and low speed operation, lift forces on the body become negligible and D simplifies to a diagonal matrix of quadratic and linear drag terms.

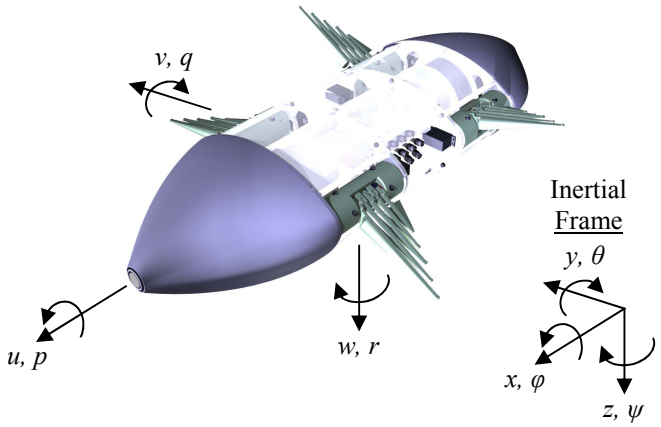

Fig. 1. Gen2 UUV design and coordinate reference frames.

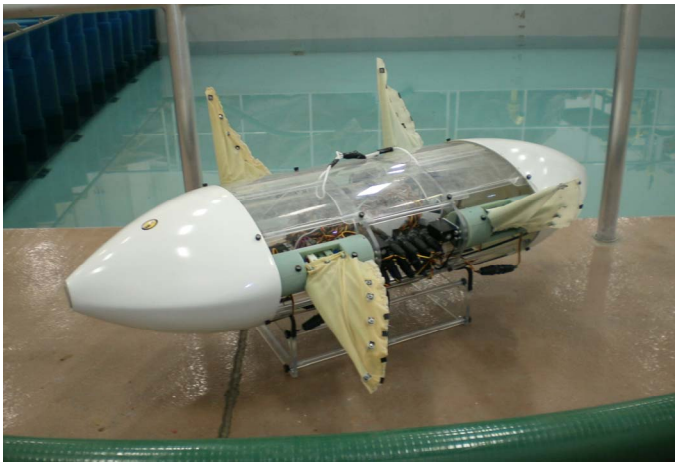

Fig. 2. Gen2 UUV prototype.

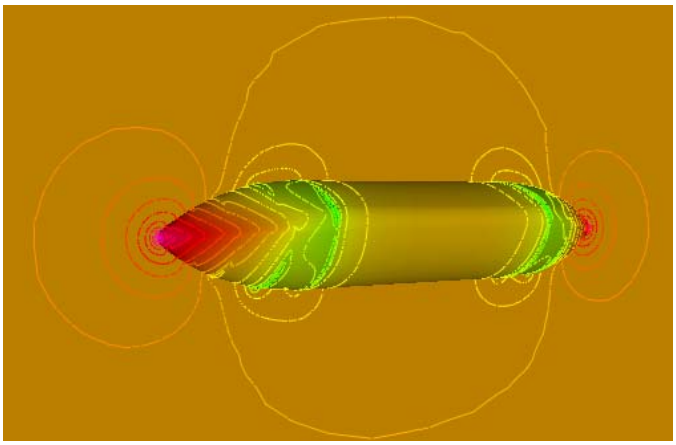

Fig. 3. Pressure contours on Gen2 vehicle hull computed using a CFD tool.

The rigid body mass terms were calculated from CAD models and physical measurements of the Gen2 vehicle. The added mass terms were calculated using strip theory as in [20][22][23]. The drag terms were computed in CFD, as illustrated in Fig. 3, and showed that the linear terms were negligible along and about all axes. Axial drag results along each body axis are shown in Fig. 4.

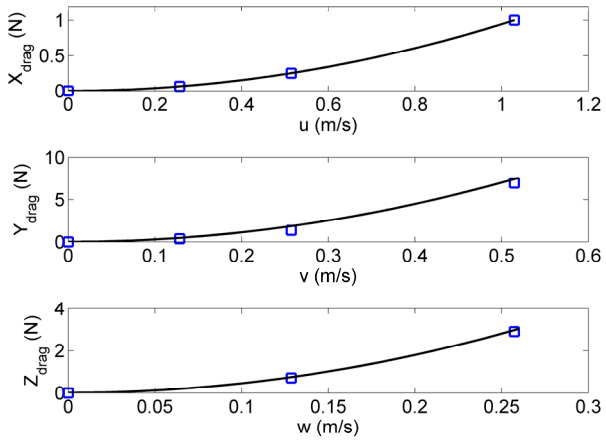

Fig. 4. Vehicle axial drag as a function of axial velocity as computed using a CFD tool.

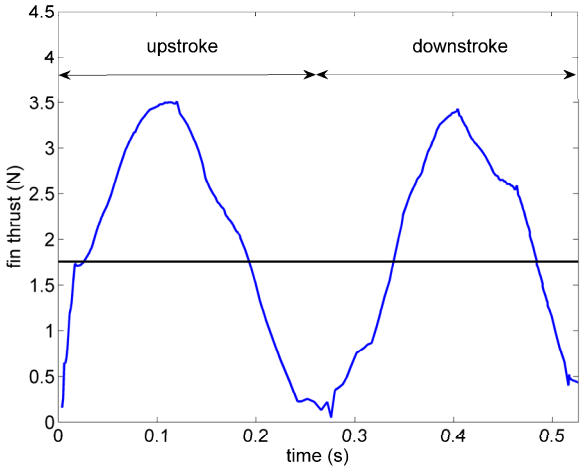

Fig. 5. CFD computed thrust time history for the Gen2 fin using experimental forward gait kinematics at 1.8 Hz flapping frequency. Average thrust is computed as 1.76 N.

C. *Fin Model*

The actively controlled curvature fins have been mounted to the rigid body of the Gen2 vehicle such that fin thrust acts along the body *x*-axis and fin lift acts along the body *z*-axis. In the current study, fin force generation along the body *y*-axis has been neglected as the differential in the force produced by the left side fins compared with the right side fins is close to zero in this direction. We then represent the forces and moments produced by the fins on the vehicle as,

$$\vec{\tau}_{fins} = \begin{bmatrix} f_{T,LF} + f_{T,LB} + f_{T,RF} + f_{T,RB} \\ 0 \\ -f_{L,LF} - f_{L,LB} - f_{L,RF} - f_{L,RB} \\ -y_L\left(f_{L,LF} + f_{L,LB}\right) - y_R\left(f_{L,RF} + f_{L,RB}\right) \\ x_F\left(f_{L,LF} + f_{L,RF}\right) + x_B\left(f_{L,LB} + f_{L,RB}\right) \\ -y_L\left(f_{T,LF} + f_{T,LB}\right) - y_R\left(f_{T,RF} + f_{T,RB}\right) \end{bmatrix} \quad (4)$$

Here f_T is fin thrust, and f_L is fin lift. Subscripts 'LF', 'LB', 'RF', and 'RB' identify the left front, left back, right front, and right back fins, respectively. The *x*-position of the center of pressure on the fins is denoted by x_F for the front fins and x_B for the back fins. The *y*-position of the center of pressure on the fins is denoted by y_L for the left fins and y_R for the right fins. The center of pressure defines the location of the fin generated forces which is needed to compute the fin generated moments, and was determined in CFD simulations [16].

Incorporating changes to fin geometry and kinematics, Gen2 fin force generation has been characterized using CFD to complement the experimental results presented in [19]. A CFD computed thrust time history for forward gait kinematics is shown in Fig. 5.

Based on the Gen2 fin thrust and lift results, we have updated the fin models from [18] to reflect the improved force generation, as well as the differences in the effects of free stream flow speed on fin thrust as shown in Fig. 6 for the forward thrust producing gait. As with the Gen1 fin and vehicle, Gen2 fin thrust decreases linearly with free stream flow speed in the regime of flow speeds the vehicle is expected to experience.

The Gen2 fin kinematics selection and fin force production characterization is an active area of research, and the fin model continues to be updated as these fin studies produce results. More detailed studies of fin kinematics including curvature time histories, and flapping frequency and amplitude will lead to improved fin thrust and lift performance. This will lead to improved vehicle performance as well as a more refined fin model.

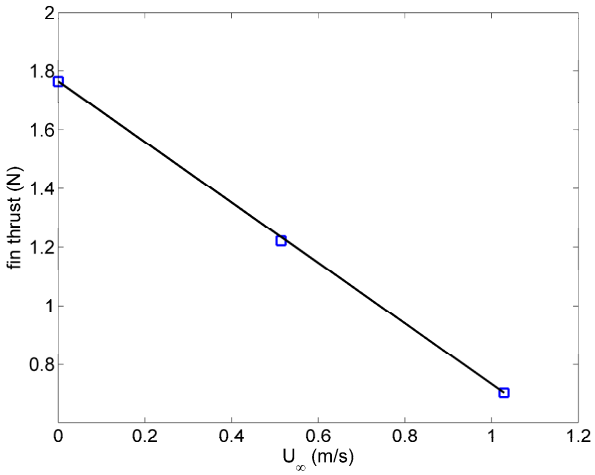

Fig. 6. CFD computed average thrust for the Gen2 fin at varying free stream flow speeds.

III. Simulation and Model Validation

The 6-DOF model of Gen2 vehicle dynamics was implemented in MATLAB and Simulink to enable simulation of vehicle performance (Fig. 7). Vehicle experiments were conducted to validate the model in heave (translation along the body z-axis) and yaw (rotation about the body z-axis) characteristics similar to the validation done for the Gen1 vehicle model [18].

A. Heave Performance

Heave performance is validated by setting an equal fin stroke angle bias for each of the four fins (to generate a downward force) and running the vehicle to a steady-state heave rate. Fin lift as a function of fin stroke angle bias has been characterized in [18], and has been adjusted for the Gen2 fin based on computational results as,

$$f_{L,\Phi_{bias}} = -0.0038 \cdot \Phi_{bias} \tag{5}$$

Here Φ_{bias} is the fin stroke angle bias. With $\Phi_{bias} = 45^{o}$ for all four-fins, each fin yields a –0.17 N lift force. At this operating point, a steady-state vehicle heave rate of 3.1 cm/s is achieved in simulation (Fig. 8). Experimental results demonstrate a steady-state heave rate of 3.3 cm/s, a difference of 6.4 % which is explained by finite sensor precision and errors in fin kinematics modeling.

B. Yaw Performance

Yaw performance is validated by setting a differential in fin curvature between the left- and right-side fins and running the vehicle to a steady-state yaw rate. Fin thrust as a function of fin curvature has been characterized in [18], and has been scaled for the Gen2 fin based on computational results as,

$$f_{T,\kappa} = \frac{-21}{8.0 - 0.10 \cdot e^{10 \cdot \kappa}} + 1.8 \tag{6}$$

Here κ is the fin curvature constant ranging from zero (full reverse gait curvature) to one (full forward gait curvature). The two fins on the left use the forward thrust gait, while the two fins on the right use the reverse thrust gait. Because the forward thrust gait generates a larger magnitude force than the reverse thrust gait, a reduction in fin curvature (60 %) is programmed into the left fins to ensure near zero net forward thrust. The resulting magnitude of average thrust from each of the four fins becomes 0.7 N.

In simulation, a steady-state vehicle yaw rate of 37^{o}/s is achieved (Fig. 9). Experimental results demonstrate a steady-state yaw rate of 41^{o}/s. This 11 % error in the model could be attributed to a number of sources including scaling assumptions in the fin thrust model and computations of the vehicle yaw rate damping constant.

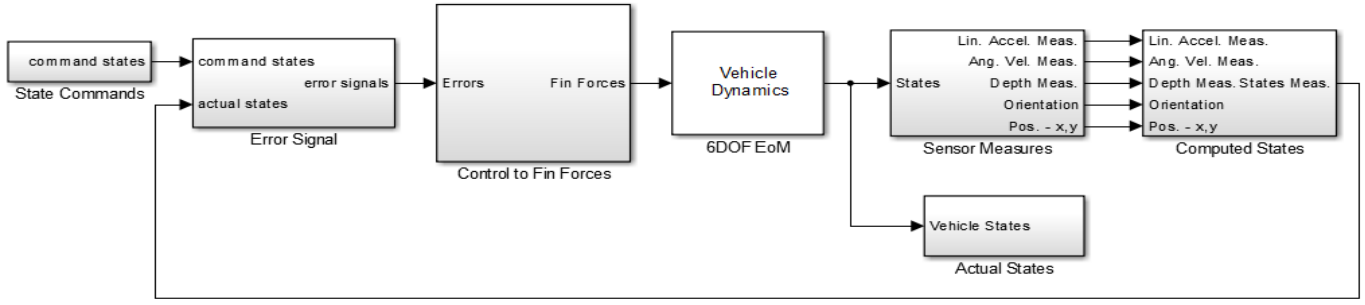

Fig. 7. Simulink block diagram for vehicle dynamics simulation showing models of fin forces, vehicle 6-DOF equations, and sensors.

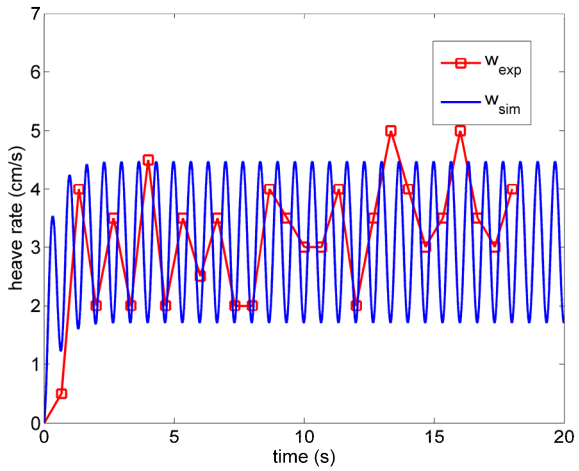

Fig. 8. Simulated and experimental open-loop heave rate response to a 45^{o} fin stroke angle bias.

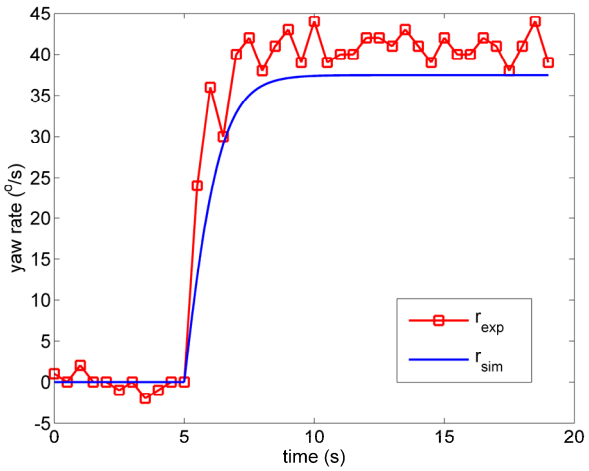

Fig. 9. Simulated and experimental open-loop yaw rate response to forward/reverse gait curvature differential between left- and right-side fins.

While validation of the 6-DOF vehicle dynamics model is not complete using only analysis of experimental heave and yaw, it does validate the methods by which vehicle dynamics coefficients are calculated. The rigid body mass, added mass, and drag coefficients validated through heave and yaw experiments were computed using the same equations and tools as the coefficients describing the other vehicle modes of motion.

IV. Closed Loop Maneuvering Performance

With a validated vehicle dynamics model, closed-loop control performance for simple maneuvers was analyzed in simulation and experiments. Vehicle control is achieved, as in [15][18], by combining preprogrammed fin gaits to alter the fin kinematics and vector thrust in a direction to produce desired vehicle motion.

A. Depth Control

Feedback of vehicle depth through a pressure transducer (SSI Technologies P51-series) provides the primary source of state information for vehicle depth control. Fin bias is controlled as a function of depth, pitch rate and angle, and roll rate and angle as in (7). As the vehicle has sufficient natural damping in heave, feedback of depth rate is not needed.

$$\begin{aligned}
\Phi_{bias,LF} &= K_z(z_{com}-z)+K_q q+K_\theta\theta+K_p p+K_\varphi\varphi \\
\Phi_{bias,RF} &= K_z(z_{com}-z)+K_q q+K_\theta\theta-K_p p-K_\varphi\varphi \\
\Phi_{bias,LB} &= K_z(z_{com}-z)-K_q q-K_\theta\theta+K_p p+K_\varphi\varphi \\
\Phi_{bias,RB} &= K_z(z_{com}-z)-K_q q-K_\theta\theta-K_p p-K_\varphi\varphi
\end{aligned} \tag{7}$$

Here each K value is a gain constant on the subscripted state variable. In a dive maneuver, pitch and roll stability are ensured while depth is controlled to a commanded value. Simulated performance of the vehicle in a simple depth change maneuver (moving vertically through a column of water) is compared with experimental results as shown in Fig. 10.

In both simulation and experiment, the Gen2 vehicle completes a 40 cm dive in 14 s. The simulated depth matches the experimental depth with an average error of 0.7 cm during this dive maneuver. However, during resurfacing (after 14 s), the simulation and experiment diverge leading to a depth error of 15 cm after 16 s of that maneuver. Explanations for this error include changes in vehicle buoyancy, as there may have been pockets of air within the wetted hull, and shifting of mass within the vehicle electronics housing leading to fin bias angle saturation to maintain pitch and roll stability.

B. Heading Control

Feedback of vehicle heading through a magnetic compass and yaw rate through a gyro provides the primary sources of state information for vehicle heading control. Fin curvature is controlled as a function of forward speed, and yaw rate and angle as in (8). While vehicle position in the *x*-*y* plane would normally also drive fin curvature, the Gen2 vehicle currently does not have an accurate positioning system in this plane.

$$\begin{aligned}
\kappa_{LF} &= K_\psi(\psi_{com}-\psi)-K_r r+K_{p,u}(u_{com}-u) \\
\kappa_{RF} &= -K_\psi(\psi_{com}-\psi)+K_r r+K_{p,u}(u_{com}-u) \\
\kappa_{LB} &= K_\psi(\psi_{com}-\psi)-K_r r+K_{p,u}(u_{com}-u) \\
\kappa_{RB} &= -K_\psi(\psi_{com}-\psi)+K_r r+K_{p,u}(u_{com}-u)
\end{aligned} \tag{8}$$

Simulated performance of the vehicle in a simple yaw maneuver (in hover) is in agreement with experimental results as shown in Fig. 11. The 180° turn is completed in 6 s in both simulation and experiment. During the entire 180° heading change and steady-state oscillation, the average error between simulation and experiment is 16°. Explanations for this error include interference in compass heading measurements due to magnetic field disturbances in the laboratory environment.

Based on the validation of the feedback controller for heading, changes made to the control algorithm gains are made to improve performance. Adding yaw rate feedback dampens the oscillations seen in the Fig. 11, as shown in Fig. 12.

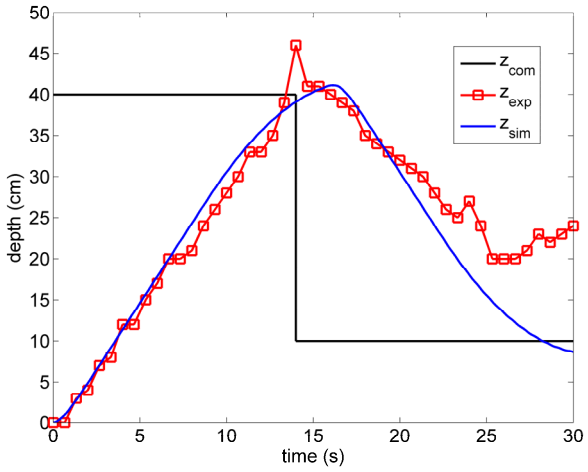

Fig. 10. Simulated and experimental closed-loop depth control (K_z = 3) response to 40 cm commanded depth change.

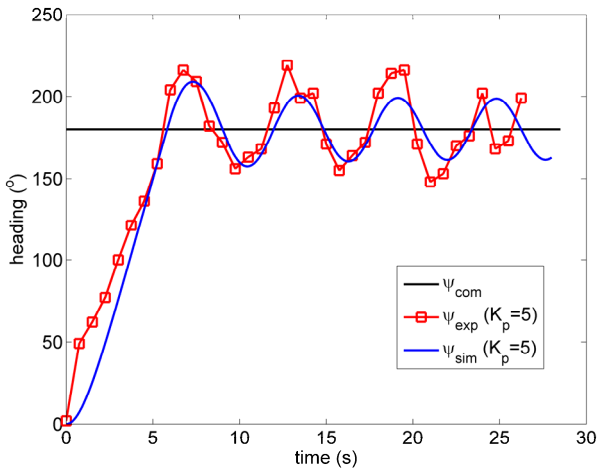

Fig. 11. Simulated and experimental closed-loop heading control (K_ψ = 5) response to 180° commanded heading change.

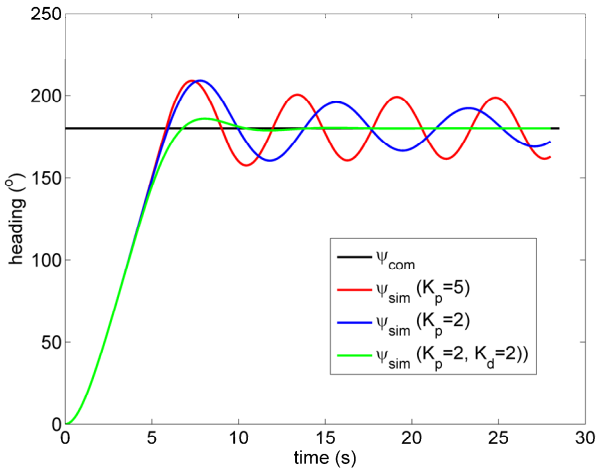

Fig. 12. Simulated closed-loop heading control comparison response to 180° commanded heading change varying heading and yaw rate control gains.

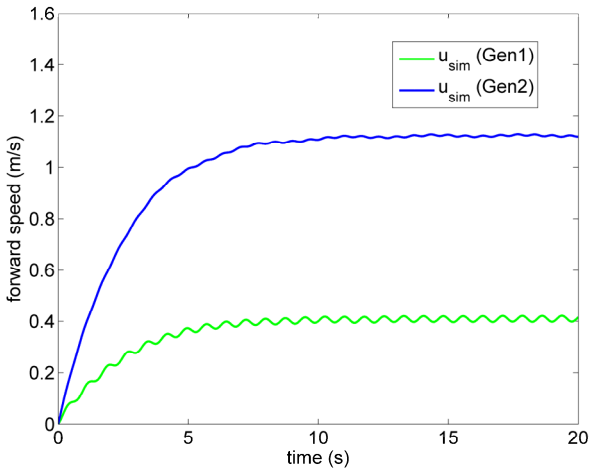

Fig. 13. Simulated open-loop comparison of Gen1 and Gen2 vehicle maximum forward speed.

V. Gen1 and Gen2 Vehicle Comparison

In addition to adding usable payload space and improving vehicle endurance, one of the main goals of creating a second generation vehicle was to improve on maneuvering performance. Based on the accuracy of the 6-DOF vehicle model presented in [18], on the scaled up fin data presented in [19], and on the simulation validation presented here, a comparison of Gen1 and Gen2 vehicle performance is made.

With respect to surge (translation along the body *x*-axis) rate, the Gen2 vehicle outperforms the Gen1 vehicle by a ratio of almost 3:1 (Fig. 13). The Gen1 vehicle was capable of a 0.41 m/s (0.79 knots) maximum forward speed [18] while the Gen2 vehicle exhibits a 1.2 m/s (2.3 knots) forward speed.

In heave and yaw, the performance of the Gen1 and Gen2 vehicles is comparable. The Gen1 maximum vehicle heave rate is 3.8 cm/s while Gen2 vehicle heave rate is 3.1 cm/s (Fig. 14). Also, the Gen1 vehicle has a maximum yaw rate of 41°/s while the Gen1 vehicle has a yaw rate of 37 °/s (Fig. 15).

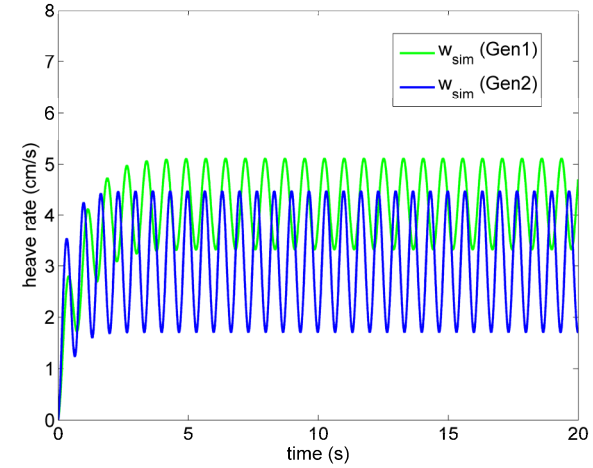

Fig. 14. Simulated open-loop comparison of Gen1 and Gen2 vehicle maximum heave rate.

VI. Discussion and Conclusions

Models of Gen2 vehicle and fin dynamics have been developed based on CFD and experimental results. Gaps in current data on the Gen2 design were extrapolated from models of the Gen1 fin [18], which will continue to be updated as results become available. However, our scaling assumptions for the vehicle and fin models yielded an accurate representation of vehicle dynamics based on comparisons of simulation and experimental vehicle results.

Open-loop vehicle responses to induced heave and yaw motion demonstrated that model performance matches experimental performance within 6.4 % in heave rate (Fig. 8) and 11 % in yaw rate (Fig. 9). Errors due to model scaling assumptions and sensor precision explain these measured differences. While model improvements will be made going forward, the current results validate our models and simulations as tools for improving vehicle propulsion and control authority.

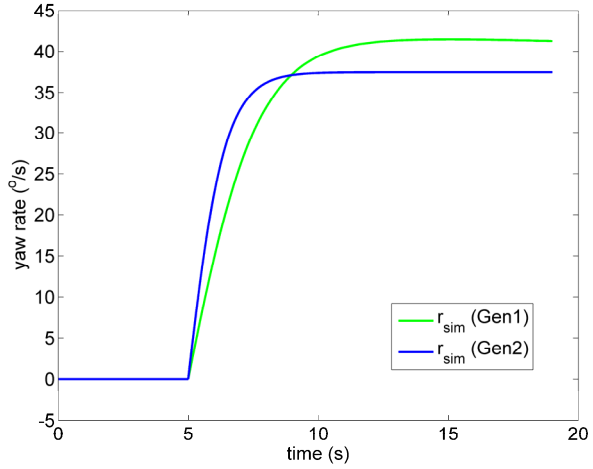

Fig. 15. Simulated open-loop comparison of Gen1 and Gen2 vehicle maximum yaw rate.

Based on experimental closed-loop performance in depth and heading control, it is evident that proportional-integral-derivative (PID) control of fin parameters is sufficient for quick and accurate simple maneuvers. This was also true with the Gen1 vehicle [18], and validates the Gen2 fins as capable effectors of propulsion and control for a highly maneuverable UUV.

While the Gen2 fins have demonstrated the capability to vector thrust in multiple directions through changes to curvature and stroke bias angle, values for these fin parameters were subjectively designed and hence preliminary. A more formal study of gait optimization for maximum thrust and lift generation is ongoing. This area of research will enable greater control authority and improved vehicle performance.

Maximum forward speed of the Gen2 vehicle has improved over the Gen1 vehicle to 1.2 m/s (2.3 knots) (Fig. 13). Operating in this range, between 2 to 3 knots, enables much greater position holding capability and vehicle control in shallow water areas.

Although improvements in surge were demonstrated, the current Gen2 vehicle performance in heave and yaw shows no improvement over the Gen1 vehicle (Fig. 14 and Fig. 15) indicating a need to improve fin kinematics and investigate fin orientation effects [17] for greater thrust vectoring authority.

In conclusion, while there will continue to be improvements in fin and vehicle modeling, the dynamics models developed and presented in this paper accurately capture the dynamics of the Gen2 vehicle prototype. Additionally, while Gen2 fin kinematics for thrust and lift production have not been optimized, the Gen2 vehicle performance shows improvement over the Gen1 vehicle primarily in surge motion. The benefits of additional payload space and reduced power consumption [19] also cannot be ignored.

REFERENCES

[1] J. E. Colgate and K. M. Lynch, "Mechanics and control of swimming: a review," IEEE Journal of Oceanic Engineering, vol. 29, pp. 660–673, July 2004.

[2] J. C. Liao, "A review of fish swimming mechanics and behavior in altered flows," Philosophical Transactions of the Royal Society B. vol. 362(1487), pp. 1973–1993, November 2007.

[3] R. W. Blake, "The mechanics of labriform motion I. Labriform locomotion in the angelfish (*pterophyllum eimekei*): An analysis of the power stroke," Journal of Experimental Biology, vol. 82, pp. 255-271, 1979.

[4] R. W. Blake, "Fish functional design and swimming performance," Journal of Fish Biology, vol. 65, pp. 1193-1222, 2004.

[5] P. W. Webb, "The biology of fish swimming," in Mechanics and Physiology of Animal Swimming, Maddock L, Bone Q, Rayner JMV (eds), Cambridge University Press, Cambridge, 1994, pp. 45-62.

[6] B. Hobson, M. Murray, and C. A. Pell, "PilotFish: Maximizing agility in an unmanned underwater vehicle," Proceedings of the International Symposium on Unmanned Untethered Submersible Technology, Durham, NH, 1999.

[7] S. Licht, V. Polidoro, M. Flores, F. S. Hover, and M. S. Triantafyllou, "Design and projected performance of a flapping foil AUV," IEEE Journal of Oceanic Engineering, vol. 29, no. 3, 2004.

[8] P. Sitorus, Y. Nazaruddin, E. Leksono, and A. Budiyono, "Design and implementation of paired pectoral fins locomotion of labriform fish applied to a fish robot," Journal of Bionic Engineering, vol. 6, pp. 37-45, 2009.

[9] N. Kato, et al., "Elastic pectoral fin actuators for biomimetic underwater vehicles," in Bio-mechanisms of Swimming and Flying, chap. 9, Springer Japan, 2008, pp. 271-282.

[10] J. Palmisano et al., "Design of a biomimetic controlled-curvature robotic pectoral fin," IEEE International Conference on Robotics and Automation, Rome, Italy, 2007.

[11] K. W. Moored, W. Smith, W. Chang, and H. Bart-Smith, "Investigating the thrust production of a myliobatoid-inspired oscillating wing," 3rd International CIMTEC Conference, Acireale, Italy, June 8-13, 2008.

[12] J. Tangorra et al., "The effect of fin ray flexural rigidity on the propulsive forces generated by a biorobotic fish pectoral fin," The Journal of Experimental Biology, vol. 213, pp. 4043-4054, 2010.

[13] Z. Chen, T. I. Um, and H. Bart-Smith, "Bio-mimetic robotic manta ray powered by ionic polymer-metal composite artificial muscles," International Journal of Smart and Nano Materials, vol. 3 (4), pp. 296-308, 2012.

[14] Z. Wang, Y. Wang, J. Li, and G. Hang, "A micro biomimetic manta ray robot fish actuated by SMA," IEEE International Conference on Robotics and Biomimetic, Guilin, Guangxi, China, 2009, pp. 1809-1813.

[15] J. D. Geder, J. Palmisano, R. Ramamurti, W. C. Sandberg, and B. Ratna, "Fuzzy logic PID based control design and performance for a pectoral fin propelled unmanned underwater vehicle," International Conference on Control, Automation, and Systems, Seoul, Korea, 2008.

[16] J. S. Palmisano, J. Geder, R. Ramamurti, W. C. Sandberg, and B. Ratna, "Robotic pectoral fin thrust vectoring using weighted gait combinations," Applied Bionics and Biomechanics, vol. 9, pp. 333-345, 2012.

[17] J. D. Geder et al., "Dynamic performance of a bio-mimetic UUV: Effects of fin gaits and orientation," Proceedings of the 17th International Symposium on Unmanned Untethered Submersible Technology, Portsmouth, NH, USA, 2011.

[18] J. D. Geder et al., "Four-fin bio-inspired UUV: Modeling and control solutions," ASME International Mechanical Engineering Congress and Exposition, 2011-64005, November 2011.

[19] J. D. Geder et al., "Scaling studies for an actively controlled curvature robotic pectoral fin," International Conference on Intelligent Robotics and Applications, pp. 141-150, Montreal, Canada, November 2012.

[20] T. I. Fossen, Guidance and Control of Ocean Vehicles, John Wiley & Sons, New York, 1994.

[21] W. Wang and C. M. Clark, "Modeling and simulation of the VideoRay Pro III underwater vehicle," MTS OCEANS Conference, May 2007.

[22] K. T. Patton, "Tables of hydrodynamic mass factors for translational motion", ASME Paper No. 65-WA/Unt-2, 1965.

[23] J. D. Geder, J. Palmisano, R. Ramamurti, W. C. Sandberg, and B. Ratna, "A new hybrid approach to dynamic modeling and control design for a pectoral fin propelled UUV," 15th International Symposium on Unmanned Untethered Submersible Technology, Durham, NH, 2007.